Adaptive Morphologic Regularizations for inverse problems

Pulak Purkait and Bhabatosh Chanda

ECSU, Indian Statistical Institute

Abstract. Regularization is an well-known technique for obtaining stable solution of ill-posed inverse problems. In this paper we establish a key relationship among the regularization methods with an edge-preserving noise filtering method which leads to an efficient adaptive regularization methods. We show experimentally the efficiency and superiority of the proposed regularization methods for some inverse problems, e.g. deblurring and super-resolution (SR) image reconstruction.

1 Introduction

Observed images of a scene are usually degraded by blurring due to atmospheric turbulence and inappropriate camera settings. The images are farther degraded by the various noises present in the environment and the system. Moreover, sometimes we end up with low-resolution (LR) image of the scene due to hardware limitations (e.g., sensor size) of a digital camera. Therefore, it is essential to get a sharp clean image from the noisy blurred image or to get a high-resolution (HR) image from multiple low-resolution image frames. These are called deblurring and super-resolution (SR) respectively and are classical inverse problems in image processing. In these inverse problems, the relation between the observed image Y and the desired sharp image X can be represented as [1–4]

$$Y = HX + \eta \tag{1.1}$$

where Y, X and η represent lexicographically ordered column vectors of the observed image, desired sharp image and the additive noise respectively. H is blurring matrix for deblurring problem. For SR problem, H embeds in itself geometric transformation (i.e. subpixel-shifts), downsampling and blurring [4].

The classical inverse problems (i.e., (1.1)) has been studied in both frequency and spatial domains extensively in last few decades. In frequency domain Wiener filter [5] is the most popular one that minimizes the mean square error. In spatial domain, the solution is obtained by solving an unconstrained optimization problem, such as

$$\hat{X} = \arg\min_X \{\frac{1}{2}\|HX - Y\|_2^2 + \mu\Upsilon(X)\} \tag{1.2}$$

where μ is the regularization parameter (also known as Lagrange multiplier) that controls the emphasis between the data error (first term) and the regularization (second term). $\Upsilon(X)$ mostly represent the smoothness criterion by means of energy in first or

second order image derivative. In this work we concentrate only on regularization based spatial domain iterative algorithms which solve the minimization problem (1.2).

One of the most common regularization methods for inverse problem is Tikhonov regularization [6] using bounded variation (L_2 norm). It enforces smoothness in the reconstructed image, but at the same time loses some details (e.g., edges). An edge preserving regularization method is total variance (TV) using L_1 norm of the gradients or high-frequency wavelet components [2, 3, 7]. Farsiu *et al.* [8] employed bilateral total variation (BTV) and L_1 norm for both regularization and data fusion. Recently, some other regularization terms are proposed, viz. "non-local means" (NLM) [9], "steering kernel" (SKR) [10], "Gain-controlled" [11] and "Morphologic" [4] regularization.

Even though all these regularizations lead to stable solution, an edge-preserving regularization method that can suppress noise in degraded images and the ringing artifacts evolved during reconstruction of image without sacrificing edges is yet to achieve.

In this work, our contribution is multi-fold. First, we analyze the different regularization methods and show that they all emerge from the same concept involving low-pass filtering which is basically smoothness prior. We also analyze different types of smoothness kernels and found their commonalty. Based on these studies, we develop two adaptive kernels for low-pass morphologic filter using geodesic distance between the candidate pixel and its neighboring ones. Finally, combining all these, we devise two new regularization method as a prior for inverse image restoration problems.

2 Regularizer and Filtering for inverse problems

The objective of regularization is to ensure that the reconstructed image satisfies some quality criterion. From Bayesian point of view, regularization method corresponds to imposing certain prior in estimating image. For example, regularization may ensure smoothness in the reconstructed image or may improve the rate of convergence of iterative reconstruction algorithm. Here our intention is to develop a regularization method for estimating the output image with sharp edges and textures while suppressing the noise as well as undesired artifacts.

2.1 Regularization techniques

To obtain a stable solution, suppose a specific regularization operator Υ is imposed on the estimated sharp image X. The regularization term $\Upsilon(X)$ (1.2) incorporates prior knowledge of the desired solution, e.g., degree of smoothness. A commonly used regularization term, viz, the Tikhonov cost function [6, 12–16] (sometimes called bounded variation (BV)), is given by

$$\Upsilon(X) = \|\Gamma X\|_2 \tag{2.1}$$

where Γ is usually a high-pass operator such as derivative or Laplacian. Since high-pass operators capture edges and noise with equal emphasis, minimization of $\|\Gamma X\|_2$ leads to suppression of noise along with blurring of edges. An early edge preserving regularization for inverse problems is total variation (TV) method [2, 3, 7] that penalizes

the total amount of change in the image as measured by the L_1 norm of the magnitude of the gradient, i.e.,

$$\Upsilon(X) = |\nabla X|_1 \tag{2.2}$$

Bilateral total variation (BTV) [8] combines the total variation and the bilateral filter [17, 18]. This is extension of TV regularization and is given by

$$\Upsilon(X) = \sum_{l=-w}^{w} \sum_{m=-w}^{w} \beta^{|m|+|l|} |X - S_x^l S_y^m X|_1 \tag{2.3}$$

where S_x^l and S_y^m are shift operator matrices to represent l and m pixel shift in horizontal and vertical directions, respectively, such that $l+m \geq 0$. The term w is referred to as the window size and β $(0 < \beta < 1)$ is the weighting coefficient.

Purkait *et al.* [4] proposed the regularization function based on multi-scale morphology as:

$$\Upsilon(X) = \sum_{s=1}^{S} \alpha^s \mathbf{1}^t [C_s(X) - O_s(X)] \tag{2.4}$$

where $\mathbf{1}$ is a column vector consisting of all 1's and α is the weighting coefficient. $C_s(X) = (X \oplus sB) \ominus sB$ and $O_s(X) = (X \ominus sB) \oplus sB$ are morphological closing and opening operators with disk structuring element sB of size s. Clearly, regularization operators (2.2)-(2.4) are based on some high-pass operators. Ideal regularizer is expected to capture only noise present in the image so that minimizing $\Upsilon(X)$ leads to suppression of noise while keeping sharp edges unaltered. Among above regularizers, the morphologic regularizer (2.4) is the closest to the ideal, as the open and close filters remove noise smaller than SE and preserve edges upto the curvature of SE. The edges are preserved more accurately if the costly operators opening closing by reconstruction are used. In the next section we derive a relation between smoothing filter and regularization operator.

2.2 Regularizer and smoothing kernel

Smoothing a data-set mainly creates an approximating function that captures the underlying pattern in the data, while leaving out noise or other fine-scale structures. Traditionally, people use symmetric linear filter (e.g. Gaussian filtering) or nonlinear filter (e.g. median filter). The regularization techniques described in previous section may be viewed as a *prior* which suggests that the image is composed mostly of smooth regions. That means the reconstructed image would be mostly unaffected by low pass filtering with a constraint that it satisfies the forward image generating process (data error term of (1.2)). This constraint takes care of generating high frequency components due to boundaries.

Let $K = (\alpha_{lm} | l, m = -w : w)$ be the kernel of linear low pass spatial filter. For average filter $\alpha_{lm} = 1/S$, and for Gaussian filter $\alpha_{lm} = \frac{1}{S} \exp^{-\frac{l^2+m^2}{2\sigma^2}}$, where S is the normalizing constant so that $\sum_{l,m} \alpha_{lm} = 1$. Suppose W denotes an index set incorporates an window around a pixel. As discussed in the last section, an ideal image prior would

be invariant to low pass filtering that can remove noise and keep all the image details. Then the regularization term may be defined as

$$\Upsilon(X) = \|X - KX\|_p \tag{2.5}$$
$$= \|X - \sum_{l,m\in W} \alpha_{lm} S_x^l S_y^m X\|_p \tag{2.6}$$
$$= \| \sum_{l,m\in W} \alpha_{lm}(X - S_x^l S_y^m X)\|_p \text{ (since } \sum_{l,m\in W} \alpha_{lm} = 1) \tag{2.7}$$
$$\leq \sum_{l,m\in W} \alpha_{lm} \|X - S_x^l S_y^m X\|_p \text{ (Jensen's Inequality), for } p > 1 \tag{2.8}$$

under minimization of $\Upsilon(X)$ [note that (1.2)], (2.8) is similar to (2.3). For average filtering ($\alpha_{lm} = 1/S$) with W as 4-neighborhood, $\Upsilon(X)$ becomes

$$\Upsilon(X) = \sum_{l,m\in W} \alpha_{lm} \|X - S_x^l S_y^m X\|_p = 2\|(\nabla_x + \nabla_y)X\|_p = \|\nabla X\|_p \tag{2.9}$$

which is similar to (2.2) for $p = 1$; If $\Upsilon(X) = \|(\nabla_x + \nabla_y)X\|_p$, we end up with well-known BV (Bounded variation) and TV (Total variation) regularization for $p = 2$ and 1 respectively. Moreover, if we consider a larger window, $\Upsilon(X) = \sum_{l,m\in W} \alpha_{lm} \|X - S_x^l S_y^m X\|_p$, becomes BTV regularization for $p = 1$ and $\alpha_{lm} = \beta^{|m|+|l|}$ with $\beta \in (0,1)$. Note that $\Upsilon(X)$ basically measures energy in high-frequency components. Hence, an attractive alternate regularizer could be develop using attractive derivative operators.

Spatial image filtering techniques: Most of the traditional filters use a symmetric non-adaptive kernel. Those filters are able to remove noise and artifacts present in the image, but blur edges and remove textures. Tomasi *et al.* [18] used adaptive kernel for edge preserving image smoothing, known as bilateral filtering, given by

$$\alpha_{ij,\,lm} == \exp^{-\{\frac{l^2+m^2+\lambda(X(i+l,j+m)-X(i,j))^2}{2\sigma_e^2}\}} = \exp^{-\{\frac{D_{ij,\,lm}^2}{2\sigma_e^2}\}} \tag{2.10}$$

where σ_e is the scale parameter and $X(i,j)$ is the intensity value at $(i,j)^{th}$ pixels. This kernel may also be viewed as the Gaussian of Euclidean distance $D_{ij,\,lm}$ between value of the pixels [Fig. 1]. It is still one of the state-of-art linear methods for edge preserving smoothing. Various nonlinear morphological smoothing algorithms are also available in the literature [19–22]. Lerallut et al. [19] define adaptive morphological operators, called amoeba filter, where shape of the structuring element varies from pixel to pixel, determined by thresholding the geodesic distance $D_{ij,\,lm}$ of the pixel $(i+l, j+m)$ from the center pixel (i,j) [Fig. 1]. Therefore it is clear that regularization methods used in the inverse problems (2.8) evolve from low-pass filtering. Hence, a better regularizer can be developed from more efficient adaptive nonlinear low-pass filters. Based on these observations we develop two geodesic distance based regularization methods for an inverse problem.

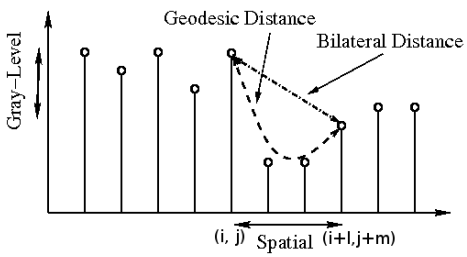

Fig. 1. Illustrates the bilateral and geodesic distances between points.

3 Proposed Morphologic Regularization

We define more general adaptive regularization as

$$\Upsilon(X) = \sum_{l,m \in W} \alpha_{lm} |\nabla^{lm}| \tag{3.1}$$

where α_{lm} is an adaptive kernel that varies from pixel to pixel. $|\nabla^{lm}| = \|X - S_x^l S_y^m X\|_p$ is p^{th} norm of the difference between the original image X and shifted one $S_x^l S_y^m X$ or $|\nabla^{lm}| = [C_s(X) - O_s(X)]$ is the norm of difference between morphologic closing and opening. In essence, a regularization term has two components: a derivative operator ∇^{lm} and a smoothing kernel α_{lm}. The elements of smoothing kernel α_{lm} decreases with distance from the candidate pixel (i, j). Morphologically viewed, an image may be considered as a topographic surface with (i, j) as spatial location and $X(i, j)$ as altitude. The geodesic distance in an image between pixels (i, j) and $(i+l, j+m)$ is defined as the length of the shortest path between them along the topographic surface. Note that BTV considers city-block distance (2.3) between pixel locations while bilateral filtering (2.10) considers Euclidean distance between two points on the topographic surface as discussed in the last section.

Based on the above study on the kernels, we can choose an efficient adaptive kernel in the following form:

$$\alpha_{ij,\,lm} = \frac{1}{S_{ij}} \exp\{-\frac{D^p_{ij,\,lm}}{2\omega^p}\} \tag{3.2}$$

where $D^p_{ij,\,lm}$ is the geodesic distance of the pixels (i, j) and $(i+l, j+m)$ within W. Based on the above geodesic kernel $\alpha_{ij,\,lm}$, We propose **geodesic regularizer** as follows:

$$\Upsilon(X) = \sum_{l,m \in W} \alpha_{lm} |X - S_x^l S_y^m X| \tag{3.3}$$

Moreover, we use adaptive morphological operators (2.4) by choosing structuring element aB adaptive instead of a flat one and is defined as

$$b_{ij,\,lm} = \delta(\alpha_{ij,\,lm} - 1), \tag{3.4}$$

where δ is an constant and is fixed over all the pixels. Accordingly the adaptive morphological dilation is defined as:

$$(X \oplus aB)(i,j) = \sup_{lm \in W} [X(i-l, j-m) + b_{(i-l)(j-m),\, lm}]. \tag{3.5}$$

And adaptive morphological erosion is defined as:

$$(X \ominus aB)(i,j) = \inf_{lm \in W} [X(i+l, j+m) - b_{ij,\, lm}] \tag{3.6}$$

Based on the above adaptive morphological operators, we also propose **adaptive morphologic regularizer** as follows:

$$\Upsilon(X) = \sum_{l,m \in W} \alpha_{lm} |C_a(X) - O_a(X)| \tag{3.7}$$

where $C_a(X)$ and $O_a(X)$ are adaptive closing and opening operators.

The energy due to different regularization terms (proposed as well as state-of-the-arts) for a noisy image are displayed in Fig. 2. It is clear from the image that proposed geodesic and adaptive morphologic regularization term extract more of noise than edges of the image.

Geodesic Distance computation

There are two main kinds of algorithms that exist in the literature for computing Geodesic distance: raster-scan and wave-front propagation. Raster-scan algorithms are based on kernel operations applied sequentially over the image in multiple passes [23]. Those methods are the extensions of Dijkstra algorithm for two dimensional grids. Wave-front algorithms such as Fast Marching Method (FMM) [24], on the other hand, are based on the iterative propagation of a pixel front with certain velocity.

Most of the existing geodesic distance computation techniques are developed for generating a distance transformation map for a gray-level image over a binary image. Whereas, in the present work, we need to compute the geodesic distance of every pixel within W from the central pixel. So here, we develop an efficient two-pass iterative raster-scan algorithm which is an extension of Dijkstra algorithm. Let $\Pi(ij,lm) = \{(i,j) = x_1, x_2, \ldots, (i+l, j+m) = x_n\}$ be a path in a connected domain between the pixels x_k and x_{k+1}. Then the geodesic distance between them is defined as:

$$D_{ij,\, lm} = \min_{\Pi} \left[\sum_{k=1}^{n-1} \{1 + \gamma |X(x_i) - X(x_{i+1})|\} \right] \tag{3.8}$$

The factor γ weights the contribution of the intensity difference against the spatial distances. Equation (3.8) generalizes the conventional spatial distance which may be obtained by setting $\gamma = 0$.

We define derivative operator

$$\nabla_{ij}^{lm} = |X(i,j) - X(i+l, j+m)|_1, \text{ where } l,m \in \{-1,0,1\} \tag{3.9}$$

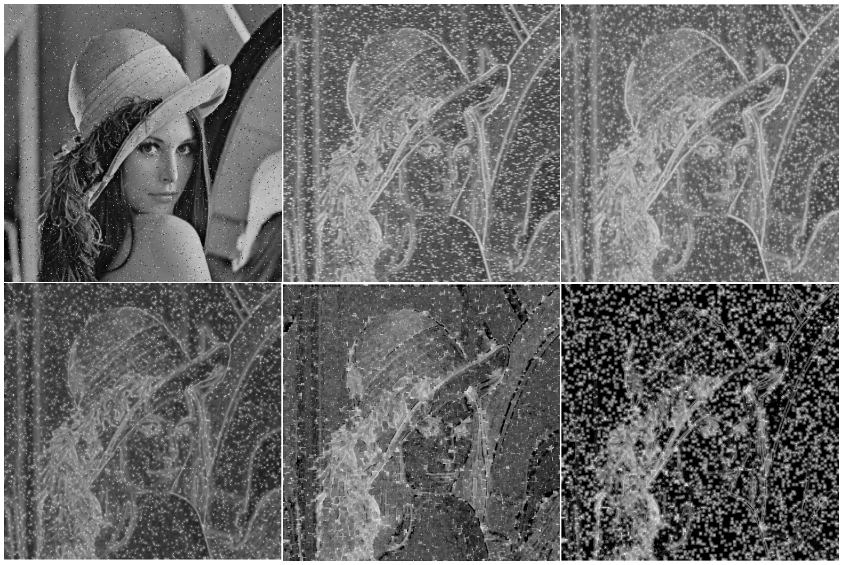

Fig. 2. Illustrates different regularization methods. Top row: noisy input image with salt and paper noise (2%), TV regularization term (2.2) and BTV regularization (2.3). Bottom row: deblurred image using geodesic regularization (3.3), Morphologic regularization (2.4), and Adaptive morphologic regularization (3.7) method. (Quantitative comparisons are in text).

Then $\gamma\nabla_{ij}^{lm} + s$ is the geodesic distance of the $(i,j)^{th}$ pixel from $(l,m)^{th}$ neighboring pixel, where s represents the cost of unit step in spatial direction. We take $s = 1$ for horizontal and vertical neighboring pixels and $s = \sqrt{2}$ for diagonal ones. The parameter γ controls the emphasis between spatial and spectral distances. Let Geo_{lm} represents geodesic distance from current $(i,j)^{th}$ pixel to $(i+l, j+m)^{th}$ pixel. We describe the computation of geodesic distance in concise algorithmic format as follows.

Algorithm

For central pixel (i, j), initialize $r = 0$**,** $Geo_{ij} = 0$
While r $<$ w iterate Pass I and Pass II.

- **Pass I** : Compute interim geodesic distances of the pixel (l,m) on the $(r+1)^{th}$ layer from the central pixel along the possible shortest paths through the inner r^{th} layer.
  - Let $N_{lm}^{(r)}$ be the neighborhood of (l,m) consisting of adjacent pixels on the r^{th} layer as shown in figure 3 and consider it as a flat adaptive structuring element at (l,m).

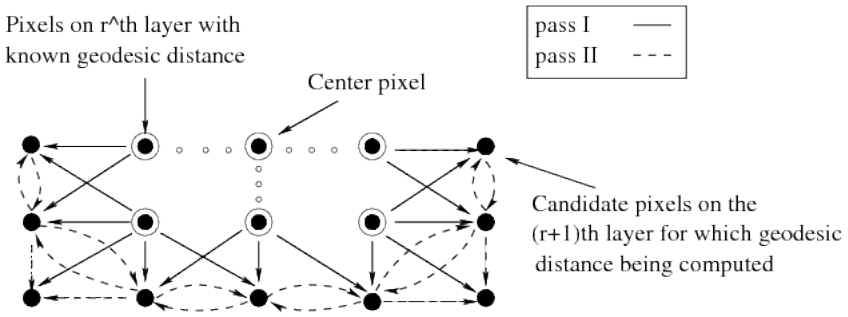

Fig. 3. Flow chart of computation of geodesic distance of a pixel to its neighboring pixels

- Interim geodesic distance of pixel (l,m) from the center of the window by eroding with $N_{lm}^{(r)}$ as

$$Geo_{lm}^{tmp} = \min_{(u,v)\in N_{lm}^{r}} \{Geo_{uv} + \gamma \nabla_{lm}^{uv} + s\}$$

– **Pass II** : Compute actual geodesic distance of the pixel (l,m) on the $(r+1)^{th}$ layer using interim geodesic distances from Pass I.
- Let $N_{lm}^{(r+1)}$ be the neighborhood consisting of adjacent pixels in the $(r+1)^{th}$ layer as shown in figure 3 and consider it as a flat adaptive SE at (l,m).
- Actual geodesic distance of pixel (l,m) from the center of the window by eroding with N_{lm}^{r+1} as

$$Geo_{lm} = \min \left[Geo_{lm}^{tmp}, \min_{(u,v)\in N_{lm}^{(r+1)}} \{Geo_{uv}^{tmp} + \gamma \nabla_{lm}^{uv} + s\} \right]$$

Now, we can compute kernel matrix $K = [\alpha_{ij,\,lm}]$ as in (3.2) with $D_{ij,\,lm} = Geo_{lm}$.

We solve (1.2) with the proposed adaptive regularization (3.1) by gradient descent technique. The non-differentiability and nonlinearity are handled by appropriate shrinkage operators [4]. The detail of optimization method is not included in this paper.

4 Experimental Results and discussion

In this section we study the performance of the proposed regularization along with some state-of-the-arts regularization methods for two classical inverse problems (i) Deblurring and (ii) Super Resolution.

Experimental Setting For quantitative evaluation purpose, we have applied each algorithm on different sets of images with different parameters and the best result of each algorithm is chosen as the output of the algorithm. To compute geodesic kernel we have chosen $\omega = 5$ and $\gamma = 0.5$. We choose 512×512 gray-scale Lena image as test image with Gaussian blurring kernel ($\sigma_b = 2.5$) plus the Gaussian noise ($\sigma_a = 5$).

Experiment I: Deblurring We synthesize a noisy blur image and then reconstruct the sharp image from it using the proposed regularization method as well as existing regularization methods. Experimental results are shown in figure 4. It is seen that the morphological regularization yields better quality reconstructed images compared to other regularization methods. Caption of figure 4 also provides the quantitative measure of quality of proposed geodesic regularization (3.3) (PSNR = 29.97dB, SSIM = 0.9228) and Adaptive morphologic regularization (3.7) method (PSNR = 30.10dB, SSIM = 0.9251) and that of Rudin *et al.* [3] (PSNR = 29.93dB, SSIM = 0.9224), Farsiu *et al.* [8] (PSNR = 29.95dB, SSIM = 0.9224), and Purkait *et al.* [4] (PSNR = 30.05dB, SSIM = 0.9248) which are the closest competitors (also state-of-art methods in this field).

Fig. 4. Illustrates results of deblurring technique with various regularization methods. Top row: noisy and blurred input image, TV regularization [3] and BTV regularization [8]. Bottom row: deblurred image using geodesic regularization, Morphologic regularization [4], and Adaptive morphologic method. (Quantitative comparisons are in text).

Experiment II: Super Resolution Reconstruction We synthesize 10 noise-free LR images down-sampled by resolution factor 5, and having different sub-pixel shifts. Then reconstruct HR image from those 10 LR images using the proposed regularization method as well as some existing regularization methods. Experimental results are shown in figure 5. It is seen that the morphological regularization yields better quality SR reconstructed images compared to other regularization methods. Caption of fig-

ure 5 also provides the quantitative measure of quality of proposed geodesic regularization (3.3) (PSNR = 29.48dB, SSIM = 0.9082) and adaptive morphologic regularization (3.7) method (PSNR = 29.59dB, SSIM = 0.9107) and that of Rudin *et al.* [3] (PSNR = 29.43dB, SSIM = 0.9077), Farsiu *et al.* [8] (PSNR = 29.47dB, SSIM = 0.9080), and Purkait *et al.* [4] (PSNR = 29.55dB, SSIM = 0.9106) which are the closest competitors (also state-of-art methods in this field).

Fig. 5. Illustrates results of various SR image reconstruction techniques on Lena image. Top row : SR image using Bicubic interpolation, TV regularization [3] and BTV regularization [8]. Bottom row : SR reconstructed image using geodesic regularization, Morphologic regularization [4], and Adaptive morphologic method. (Quantitative comparisons are in text).

5 Conclusion

In this paper, we have proposed two geodesic kernel based regularization for a general inverse problem of image reconstruction. We analyze different regularization methods used in this domain and found that they come from the same concept of edge preserving non-linear smoother. We propose a new robust adaptive geodesic regularization and adaptive morphologic regularization methods that can suppress the noise more efficiently while preserving the edges. Our experimental section shows that it works quite well, in fact better than existing techniques.

The adaptive regularization method proposed here are tested for two classic inverse problems, viz, deblurring and SR reconstruction problem, but one can easily extend this work to other applications as well.

References

1. Chang, S.G., Yu, B., Vetterli, M.: Adaptive wavelet thresholding for image denoising and compression. IEEE Trans. Image Process. **9** (2000) 1532–1546
2. Beck, A., Teboulle, M.: A fast iterative shrinkage-thresholding algorithm for linear inverse problems. SIAM J. of Imaging Sciences **2** (2006) 183–202
3. Rudin, L., Osher, S., Fatemi, E.: Nonlinear total variation based noise removal algorithms. Physica D **60** (1992) 259–268
4. Purkait, P., Chanda, B.: Super resolution image reconstruction through bregman iteration using morphologic regularization. Image Processing, IEEE Transactions on **21** (2012) 4029 –4039
5. Widrow, B., Stearns, S.: Adaptive signal processing. Englewood Cliffs, NJ, Prentice-Hall, Inc., 1985, 491 p. **1** (1985)
6. Zhang, X., Lam, E.Y., Wu, E.X., Wong, K.K.: Application of tikhonov regularization to super-resolution reconstruction of brain mri image. Medical Imaging and Informatics **49** (2008) 51–56
7. Hansen, P.C., Nagy, J.G., OLeary, D.P.: Deblurring images. Fundamentals of Algorithms. Society for Industrial and Applied Mathematics (SIAM). **3** (2006) 291–294
8. Farsiu, S., Robinson, M.D., Elad, M., Milanfar, P.: Fast and robust multiframe super-resolution. IEEE Transactions on Image Processing **13** (2004) 1327–1344
9. Protter, M., Elad, M., Takeda, H., Milanfar, P.: Generalizing the nonlocal-means to super-resolution reconstruction. IEEE Transactions on Image Processing **18** (2009) 36–51
10. Takeda, H., Milanfar, P., Protter, M., Elad, M.: Super-resolution without explicit subpixel motion estimation. IEEE Transactions on Image Processing **18** (2009) 1958–1975
11. Purkait, P., Chanda, B.: Morphologic gain-controlled regularization for edge-preserving super-resolution image reconstruction. (Signal, Image and Video Processing) 1–14
12. Chan, T.F., Wong, C.K.T.: Multichannel image deconvolution by total variation regularization. In: Proceedings of SPIE, San Diego, CA, USA (1997) 358–366
13. Li, X., Hu, Y., Gao, X., Tao, D., Ning, B.: A multi-frame image super-resolution method. Signal Processing, Elsevier **90** (2010) 405–414
14. Nguyen, N., Milanfar, P., Golub, G.: Efficient generalized cross-validation with applications to parametric image restoration and resolution enhancement. IEEE Transactions on Image Processing **10** (2001) 1299–1308
15. Nguyen, N., Milanfar, P., Golub, G.H.: A computationally efficient image super resolution algorithm. IEEE Transaction on Image Processing **10** (2001) 573–583
16. Elad, M., Feuer, A.: Restoration of a single super-resolution image from several blurred, noisy, and under-sampled measured images. IEEE Transactions on Image Processing **6** (1997) 1646–1658
17. Elad, M.: On the bilateral filter and ways to improve it. IEEE Transaction on Image Processing **11** (2002) 1141–1151
18. Tomasi, C., Manduchi, R.: Bilateral filtering for gray and color images. In: IEEE International Conference on Computer Vision, New Delhi, India (1998) 836–846
19. Lerallut, R., tienne Decencire, Meyer, F.: Image filtering using morphological amoebas. Image and Vision Computing **25** (2007) 395 – 404

20. Cheng, F., Venetsanopoulos, A.: Adaptive morphological operators, fast algorithms and their applications. Pattern Recognition **33** (2000) 917 – 933
21. Soille, P.: Generalized geodesy via geodesic time. Pattern Recognition Letters **15** (1994) 1235 – 1240
22. Debayle, J., Pinoli, J.C.: General adaptive neighborhood image processing. J. Math. Imaging Vis. **25** (2006) 267–284
23. Borgefors, G.: Distance transformations in digital images. Comput. Vision Graph. Image Process. **34** (1986) 344–371
24. Sethian, J.A.: Fast marching methods. SIAM Review **41** (1999) 199–235